JOURNAL OF MATERIALS SCIENCE 14 (1979) 945–952

Small-angle X-ray scattering study on the structure and crystallization of amorphous Fe-P-C alloy

KOZO OSAMURA, KAZUHISA SHIBUE, PAUL HIDEO SHINGU, YOTARO MURAKAMI
School of Metallurgy and Materials Science, Kyoto University, Sakyoku, Kyoto 606, Japan

The change in structure of an amorphous Fe–P–C alloy during ageing was examined using small-angle X-ray scattering (SAXS) measurement and transmission electron microscopy. The SAXS intensity was related to two different types of scattering regions depending on ageing time and temperature. The major scattering was from the crystalline particles, which had two-phase lamella structures. The average thickness of the lamellae remained constant at about 5 nm during ageing. The interlamella distance was three to five times the lamellar thickness in the regular packing region. Another minor scattering was interpreted as being caused by the local ordering of atomic configuration in the amorphous state. The average size of the scattering region was 1.8 to 2.4 nm and quite similar to the critical range proposed by Giessen and Wagner, beyond which the short-range order disappears.

1. Introduction

The question of atomic configurations in amorphous alloys has received much attention in recent years, with particular interest being directed towards the local order in the materials. Many notable investigations have been carried out on alloy systems composed of transition metals and metalloids, Ni–P [1], Fe–P–C [2, 3], Pd–Si [4], etc.

The Fe–P–C alloy is a typical material which exhibits the amorphous state when rapidly cooled from the liquid phase. The sequence of phase transformation from amorphous to stable has been investigated by Masumoto and Kimura [5]. The process was divided into four stages containing two kinds of metastable phases. Rastogi and Duwez [6] suggested that the initial crystalline phase was Fe_2P. Field ion microscope observation [7] shows that a random distribution of discernible atomic assemblies have a crystalline size of about 1 nm, on average, is observable within a random atomic matrix. Mössbauer measurements have been performed by several authors [9, 10]. Fujita *et al.* [10] proposed that the amorphous alloy has a degree of short-range order of b c c type, and during ageing between 573 and 673 K, the short-range atomic movement of metalloids, P and C, takes place. Transmission electron microscopy has been performed [5] in order to clarify the structure of as-splatted amorphous alloy as well as that of subsequently aged specimens. It was, however, difficult to determine quantitatively the nature of the inhomogeneity in materials on a fine scale in the order of several nm or less. It was found in other alloy systems (Pd–Au–Si [11] and Fe–Ni–P–B [12]), that small-angle X-ray scattering (SAXS) measurement is effective on such a fine scale to gain quantitative information concerning the size, distribution and character of the scattering regions.

In the present work, we carried out SAXS intensity measurements as well as the transmission electron microscope (TEM) observation for an Fe–P–C amorphous alloy and analysed the results in order to obtain structural information in the amorphous state and during the crystallization process.

2. Experimental methods

A drum technique was used to make the amorphous alloys. Molten alloys were ejected from the orifice of a fused silica tube and quenched rapidly by the rotating drum. Long ribbons, 15 to 25 μm thick and 2 mm wide, were obtained. The chemical composition of the prepared ribbon was chemically analysed to be Fe–10.4 at.%P–6.3 at.%C. The specimen was wrapped in aluminium foil for short-time ageing and put into evacuated fused silica ampoules for long-time ageing. The isothermal annealing was done between 613 and 763 K for up to 10 000 min, where the crystallization temperature for this alloy was about 703 K.

For TEM observation, the samples were electrolytically thinned in an electrolyte consisting of 10% perchloric acid and 90% ethyl alcohol. The specimen was polished on both sides simultaneously until a small hole was formed. The temperature of the electrolyte was maintained at -5° C or less. The thinned specimens were examined in a JEOL-120 transmission electron microscope.

The SAXS intensity for the amorphous alloys was measured in transmission geometry with a Kratky camera, of which the entrance slit was 40 μm and the scattering and receiving slits were 0.3 and 0.1 mm, respectively. The distance between the detecting plane and the specimen was 326 mm. Mo radiation was generated by a Rigaku power supply RU200PL operated at 50 kV and 160 mA. The incident beam was monochromated by a 0.04 mm Zr filter. A scintillation counter in conjunction with a single-channel analyser and scaler was used to detect the scattering intensity in the angular range between 0.05 and 7 degrees. The height of the beam was made sufficiently large so that the beam could be considered to be infinitely large. Specimens were obtained from a part of the amorphous ribbon with a thickness of 20 ± 1 μm.

In order to obtain the correct intensity, special care was taken to determine the background intensity. In the present apparatus, a weak angular-dependent intensity was observed even for fully annealed pure Fe. Its intensity was concluded to arise from air-scattering and other incidental scattering, but not connected with fluorescence and Compton scattering in the present small-angle region. Therefore, the scattering intensity from pure Fe with the same thickness was adopted as the background intensity after absorption correction. The measured intensity $\tilde{J}(s)$ was desmeared using a computer program. The desmeared intensity, $I(s)$, was then placed on an absolute basis by comparison with the scattering intensity measured for a known standard material under similar conditions. The standard material used for this purpose was a polyethylene.

3. Experimental results

The angular-dependence of SAXS intensity for the aged specimens at 763 K is shown in Fig. 1. After a short ageing of 2 min the intensity became very large and on further ageing increased in the lower scattering angle region, but decreased slightly in the higher-angle region, where the angular dependence of the intensity is recognized as strictly obeying Porod's law, namely the intensity is proportional to s^{-3}. This angular-dependence indicates a sharp interface between particle and matrix. In such a way, at temperatures above the crystal-

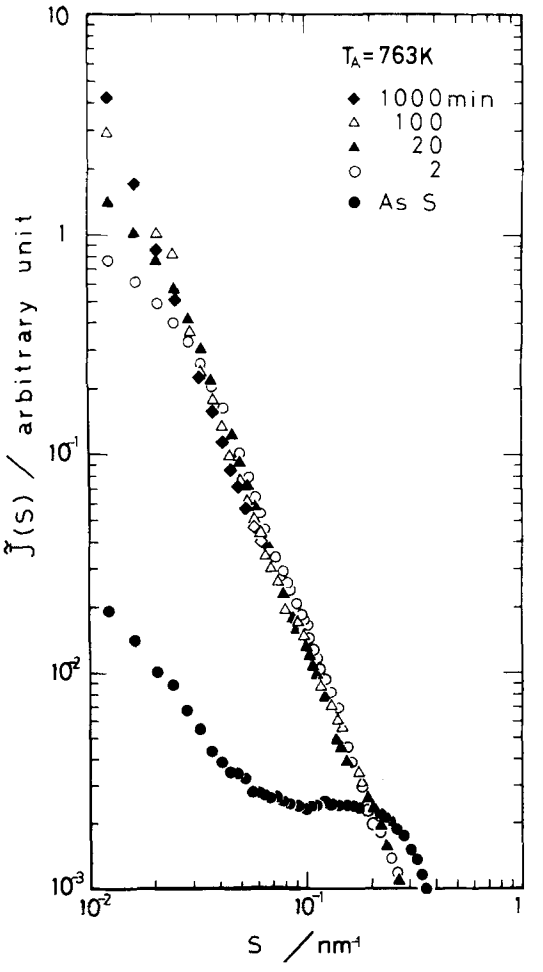

Figure 1 SAXS intensity as a function of inverse Bragg spacing for the amorphous alloys aged at 763 K, where s represents $2 \sin \theta/\lambda$ and 2θ is the scattering angle.

lization temperature, some of the nuclei grow suddenly into crystals. The Guinier radius changed gradually from 9.8 to 12.5 nm during ageing for 2 to 1000 min at 763 K.

Fig. 2 shows the scattering intensity for specimens aged for various periods at 663 K, which is lower by about 20 K than the crystallization temperature. The intensity in the specimen aged for 200 min decreased monotonically with increasing scattering angle, but at a high angle a shoulder appears in the intensity curve. For specimens aged for longer periods, the shoulder grew during ageing up to 1000 min. The scattering intensity seemed to be divided into two parts. A first part appears in the relatively lower scattering angle region with a characteristic of monotonically decreasing intensity (as presented typically in the cases of as-splatted and 50 min ageing specimens) and this part remained nearly constant during ageing. The second part, corresponding to the shoulder mentioned above, appeared in the high scattering angle region and increased with ageing time. Above 2000 min ageing, the angular-dependence of the scattering intensity was similar to those specimens aged at 763 K shown in Fig. 1. The TEM observation was performed on the same specimens used for the SAXS measurement. Fig. 3 shows the typical structures which appeared during ageing at 663 K. At 50 min, the structure remained in the amorphous state and was the same as that for the as-splatted specimen, although the SAXS intensity changed discernibly. The crystalline phase appeared in the specimen aged for 200 min. Each crystalline particle exhibited a lamellar structure and was very

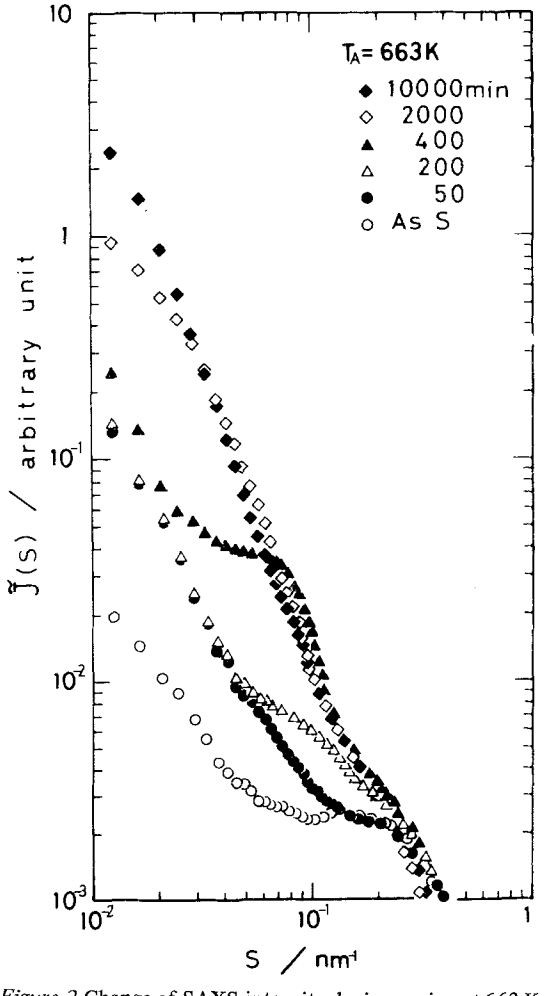

Figure 2 Change of SAXS intensity during ageing at 663 K.

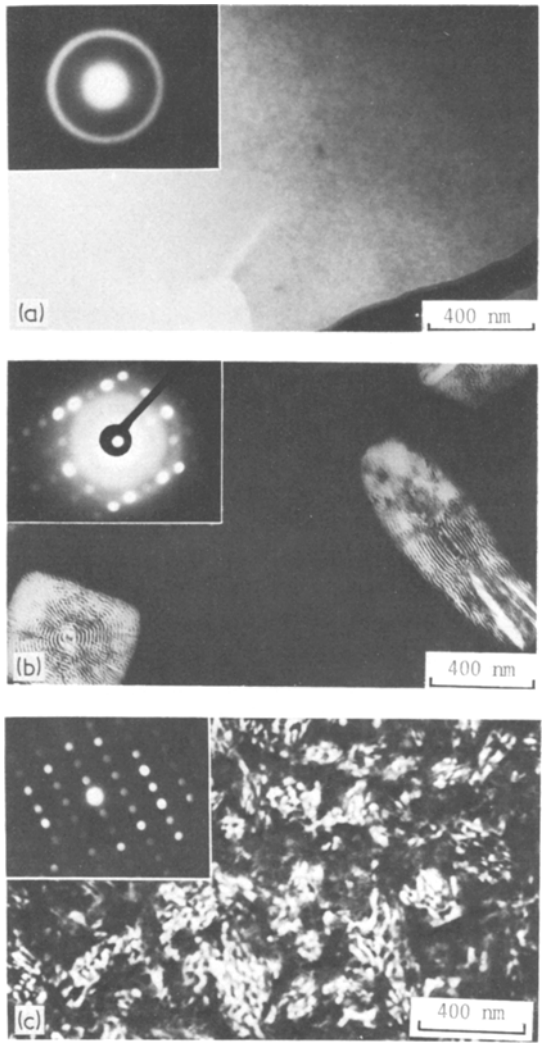

Figure 3 Structure change of an Fe–P–C amorphous alloy aged at 663 K, for (a) 50 min; (b) 200 min; and (c) 2000 min. The diffraction pattern of (b) arose from the central area of the long particle located at the right-hand side.

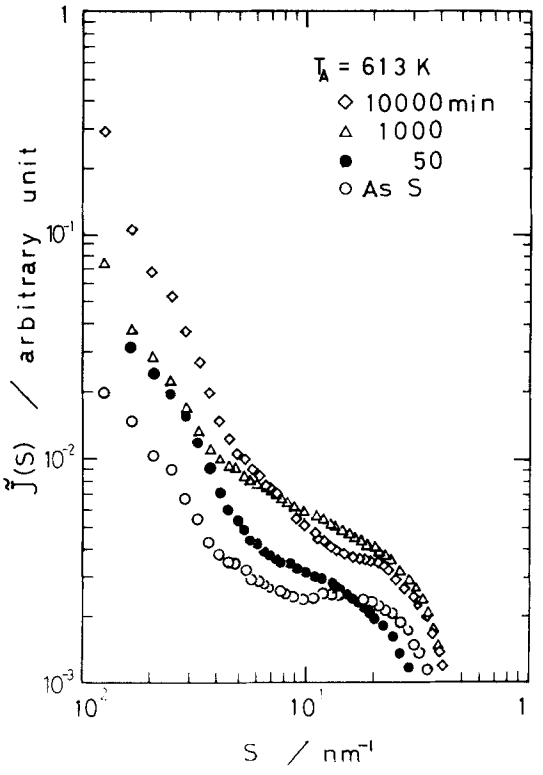

Figure 4 Change of SAXS intensity during ageing at 613 K.

similar to an "axialite" grown from polymer fluid [13]. The appearance of the axialite corresponded to the shoulder found in the SAXS intensity profile. After ageing for 2000 min, phase separation occurred over the entire specimen and its structure became rather irregular.

The SAXS measurement was also performed for the specimens aged at 643 K, where the axialites were observed in the specimens aged for 5000 and 10 000 min. The ageing behaviour of intensity profiles against scattering angle was quite similar to that for the cases at 663 K except that the appearance of the shoulder was delayed during ageing.

When the amorphous alloy was aged at 613 K, no crystalline phase was observed even on ageing for 10 000 min. The SAXS intensity increased gradually during ageing as shown in Fig. 4, suggesting the occurrence of some atomic configuration change within the amorphous state.

For X-ray diffraction in materials, the density–density correlation is given by the equation [14]

$$\gamma(\vec{r}) = \int_v \Delta\rho(\vec{r}_1)\,\Delta\rho(\vec{r}_1 + \vec{r})\,\mathrm{d}\vec{r}_1, \qquad (1)$$

where $\Delta\rho(\vec{r})$ is the fluctuation of electron density at position $\vec{r}$. The above function will simply be called the "correlation function" hereafter. When a centre of symmetry exists, the correlation function can be directly obtained from the observed intensity, $I(s)$ without any assumption as follows:

$$\gamma(r) = \frac{1}{2\pi^2 r}\int_0^\infty sI(s)\sin(sr)\,\mathrm{d}s. \qquad ((2)$$

It is noted that the present correlation function is different by a factor of $8\pi^3$ from the Q-function defined by Hosemann [15]. At $r = 0$, the function has a special meaning and is usually called the "integrated intensity",

$$\gamma(0) = \frac{1}{8\pi^3}\int_0^\infty 4\pi s^2 I(s)\,\mathrm{d}s$$
$$= \langle\Delta\rho^2\rangle V_f(1 - V_f) \qquad (3)$$

where $\langle\Delta\rho^2\rangle$ is the square mean fluctuation of electron density over the whole system and V_f is the volume fraction. Fig. 5 shows the experimental results for some aged specimens. In the specimens aged for 10 000 min at 663 K and for 100 min at 763 K, in which the crystallization was completed and two crystalline phases exist, the correlation was very strong and reached 20 nm or more. On the other hand, in the specimens aged for 2000

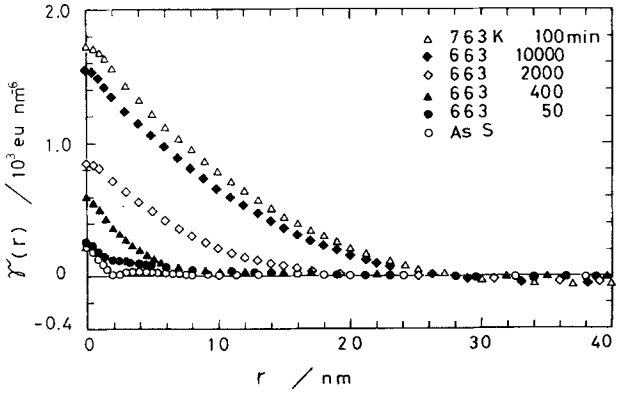

Figure 5 Density–density correlation as a function of radial distance for specimens aged at various temperatures.

min at 663 K and the as-splatted specimen, which have an amorphous structure, the correlation was very weak and became nearly zero at the further radial distances.

4. Structure of the crystalline phase

The crystalline phase, which appeared firstly from the amorphous state, had a lamellar structure as shown typically in Fig. 3b. One of the alternate phases was confirmed to be Fe_3P, from analysis of a diffraction pattern. The structure of the other phase was not determined, but weak spots of α-Fe were often observed in the same diffraction area for the other specimens aged for longer periods. The three-dimensional structure of these crystalline particles deducible from the observed two-dimensional pictures was the cylindric accumulation of fine lamellae. The regular packing existed only locally and did not occur over the entire particle. A sketch of such regularly piled lamellae is shown in Fig. 6, where D is the thickness of lamellae and L is the average interlamellar distance. When it was assumed that the closest packing of lamellae occurs in the x-direction and the dimensions of the other (y and z) directions are fairly large, the two parameters, D and L, could be determined from two different types of analysis of SAXS intensity as given below.

According to Porod [16], the scattering intensity from the one-dimensional lamellar packing, where the central separation of neighbouring lamellae with an equal thickness, D, has a Gaussian fluctuation, is given by

$$I(s) = \frac{2k(L-D)}{D}\frac{1}{s^2} \times \frac{1-\cos(sD)}{[1-\cos(sD)]^2 + [s(L-D)+\sin(sD)]^2}, \quad (4)$$

where k is a constant. The term $1/s^2$ indicates the contribution from the other two directions, y and x, under the limitation of a sufficiently high scattering angle. Fig. 7 shows the calculated relative change of $s^2I(s)$ based on the structural model shown in Fig. 6 as a function of $sD/2\pi$ for some cases with different L/D ratios. In the same figure, the calculated result based on an observed SAXS intensity distribution was plotted. The experimental data corresponded well with the calculated curve for $L/D = 17.0/5.0$. The broadened angular-dependence of the experimental data are suggested

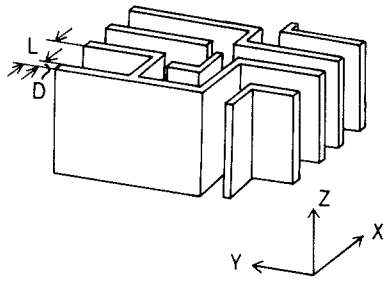

Figure 6 Proposed structure of the initially crystallized phase, where lamellae with a thickness D are piled densely along the x-direction and L is the average lamellar spacing.

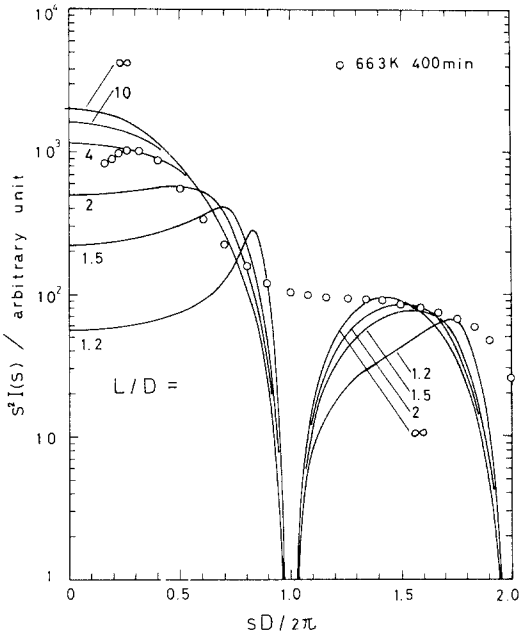

Figure 7 Relative change of $s^2I(s)$ as a function of $sD/2\pi$, where solid curves are the theoretical results calculated from Equation 4 with various L/D values and open circles are the observed data fitted to the theoretical curve by changing the intensity scale.

to result from a distribution of thicknesses of lamellae and from the irregularity of lamellar packing. As shown in Fig. 8, such a characteristic angular-dependence always appeared for those specimens in which the axialite was observed by TEM observation. The analytical results are listed in Table I.

The observed correlation function for these specimens is shown in Fig. 9. Their radial dependence of correlation was very similar to each other. The correlation decreased rapidly at first near the origin and had a weak broadened maximum in the region of 10 to 20 nm. For a lamella with thick-

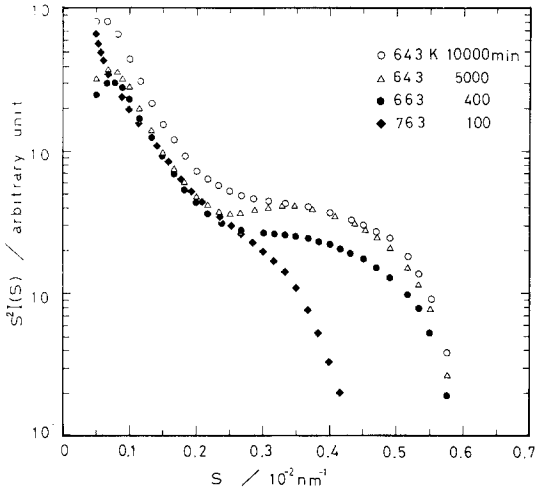

Figure 8 Observed values of $s^2I(s)$ versus inverse Bragg spacing for specimens aged at various temperatures.

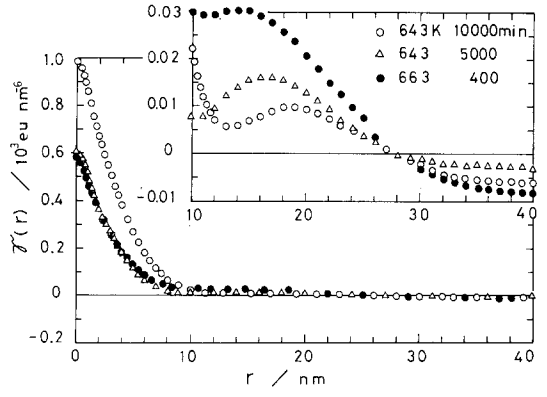

Figure 9 Density–density correlstion in the aged specimens containing fine particles of the crystalline phase.

ness D, the correlation function is represented as

$$\gamma(r) = \langle \Delta\rho^2 \rangle D\left(1 - \frac{r}{D}\right). \qquad (5)$$

From the slope near the origin, the average thickness of lamellae was obtained. The distance to the maximum gave an average nearest neighbour distance L among lamellae. As seen from Table I, the present results matched fairly well the calculations obtained from Porod's theory. From TEM observations, the smallest D and the closest L were determined to be about 4 and 13 nm, respectively.

5. Structural information on the amorphous state

From TEM observation, the structure was found to remain entirely in the amorphous state up to ageing times of 100 min at 663 K, 1000 min at

TABLE I Summary on the structure of the initially crystallized phase, where D and L are the lamellar thickness and inter-lamellar spacing, respectively

Ageing conditions		From Porod's theory		From correlation function	
Temp. (K)	Time (min)	D (nm)	L (nm)	D (nm)	L (nm)
663	400	5.0	17.0	5.1	14.4
643	5000	4.5	14.0	4.6	16.6
643	10000	4.8	22.0	6.0	18.6

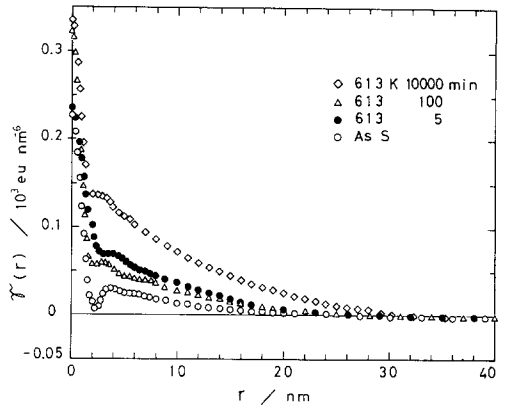

Figure 10 Density–density correlation in amorphous alloys aged at 613 K.

643 K and 10 000 min or more at 613 K. Halo diffraction was observed to be common to all the specimens. A "salt and pepper" background structure was sometimes observed in the dark-field. The size of this structure, which related to coherently diffracting domains, was not determined because of the limitation of resolution, but was qualitatively several nm or less; in addition, it could not be concluded whether or not its dark-field structure corresponds to the weak SAXS intensity.

A typical change of correlation function during ageing of the amorphous phase prior to crystallization is shown in Fig. 10. The integrated intensity, $\gamma(0)$, increased gradually during ageing. The radial distance corresponding to zero correlation was determined by extrapolating the slope near the origin, to yield an average dimension of the scattering region. Its value was 1.8 nm for the as-splatted specimen, and remained nearly constant at 2.0 to 2.4 nm for the aged specimens. After the rapid decrease of correlation near the origin, a rather weak long-distance correlation was established and increased during ageing. This means that the scattering region causing the SAXS intensity had no spherical symmetry or no distinct boundary. It should, however, be noted that no negative

correlation appeared around the origin as expected in the case of spinodal decomposition.

A quantitative estimation of density fluctuation will here be performed from the integrated intensity. When phase separation arose entirely during ageing at high temperature, three crystalline phases were confirmed [5]: α-Fe, Fe_3C and Fe_3P. The electron densities for these phases were 2.20, 2.17 and 2.01×10^3 eu nm^{-3}, respectively. The electron density for the amorphous structure was estimated to be 2.11×10^3 eu nm^{-3} averaged by multiplying the occupied volume of each phase. When a small particle of the crystalline phase, Fe_3P or α-Fe precipitated in the amorphous matrix, the difference of electron density was 0.10 or 0.09×10^3 eu nm^{-3}. For the specimen aged at 613 K for 10 000 min, which remained in the amorphous state, the integrated intensity was 0.335×10^3 eu nm^{-6} as shown in Fig. 10. If the crystalline particle precipitates, the volume fraction is calculated as 0.023 for Fe_3P and 0.041 for α-Fe. These values of volume fraction are too small to explain the long-distance correlation shown in Fig. 10. On the other hand, when the fluctuation is spread over the entire specimen, namely, $V_f = 0.5$, the difference in electron density is estimated to be 0.036×10^3 eu nm^{-3}. The relative fluctuation $\Delta\rho/\rho$ is about 1.7%. Such a small fluctuation in electron density might be explained by an inhomogeneous variation of density in the amorphous structure.

6. Discussion

It was clearly seen from the SAXS data that the amorphous alloy Fe–P–C contains two different scattering regions. The major one corresponds to scattering from the crystalline particles. The minor one, which appeared mainly during early ageing at lower temperatures as well as in the as-splatted specimen, was recognized as a kind of precursory substructure occurring prior to crystallization. A more quantitative discussion about the structure of amorphous alloys on the basis of the present results will be given later.

According to the temperature–time–transition diagram of the $Fe_{80}P_{13}C_7$ alloy reported by Masumoto and Kimura [5], the present crystalline phase, for example, which appeared after ageing at 663 K for 400 min, should correspond to MS II. However, the present phase is in dimension and structure quite different from both MS I and MS II. Perhaps it is possible for the transformation sequence to follow another path, because the alloy composition contains less Fe than that examined by the earlier authors [5]. The morphology of the present crystalline phase was very similar to the crystals observed in the alloy Ni–Fe–P–B by Walter *et al.* [17]. They reported that in the early stage of crystallization, the crystals were single phase and consisted of a collection of twinned plates and spheroids about 10 nm across. On the other hand, the present crystalline material was suggested to have a two-phase structure with different compositions, because the SAXS intensity was explained well by this two-phase fine structure, as discussed in the previous section.

In the specimens aged at relatively low temperatures as well as the as-splatted specimen, a weak diffuse scattering was observed prior to precipitation of the crystalline phase. As seen in the previous section, the central scattering region causing SAXS intensity had a dimension of 1.8 to 2.4 nm on average and was accompanied by a long-distance correlation reaching up to 20 nm. Since such regions should be distributed over the entire specimen, the deduced fluctuation of electron density with a minimum difference of 1.7% is small enough to be consistent with a variation of density in a local scale. Here an alternative mechanism could be suggested in order to consider the weak diffuse scattering. One is the spinodal decomposition, the appearance of which was reported in the amorphous Pd–Au–Si alloy by Chou and Turnbull [11]. But in the present Fe–P–C alloy it was concluded that the mechanism did not occur, because firstly no well-defined concentration waves were found during ageing and secondly the negative correlation did not appear.

The most possible mechanism is the local ordering of atomic configuration, where a movement of metalloid atoms may also occur over a short range in order to obtain a preferred co-ordination and homopolar bonding. It would be expected that an inhomogeneity of number density and a resultant change of electron density would occur locally in the matrix. As is well known [18], there are two proposed models for the amorphous structure. One is the *microcrystalline* model. From the present SAXS data, the quantitative ratio of boundary regions should be comparable to that of small randomly distributed crystallites, the external form of which has no spherical symmetry. The other model is the topological one, which is often called the *dense random packing* model. The small-

est unit is the tetrahedron consisting of a close-packed structure and these units are irregularly and continuously arranged. When this is the case, the assembly of those fundamental units should distribute randomly in space with an average size of 1.8 to 2.4 nm. Giessen and Wagner [19] defined a value r_s, beyond which the short-range order disappears. In the Fe–P–C system, r_s is 1.5 and 1.1 nm [18] for the amorphous and liquid state, respectively. Double this value is quite similar to the present average size of scattering region. However, these regions will have irregular shapes, elongating in a particular direction in space. As mentioned above, even in the limited information from the SAXS data, the topological model for the local ordering of atomic configuration was suggested to reasonably express the amorphous structure.

7. Conclusions

Above the crystallization temperature, precipitation began rapidly and tended to saturate after a short time ageing. At 763 K, the precipitated particles, which were proved to have a sharp interface, had an average Guinier radius of 9.8 to 12.5 nm during ageing for up to 1000 min.

Below the crystallization temperature, the crystalline particle, which was very similar to a polymeric axialite, appeared after an incubation period depending on the ageing temperature. It was concluded to have a two-phase lamellar structure, from TEM observation and X-ray analysis. The lamellar thickness remained constant at about 5 ± 1 nm during ageing, and the inter-lamellar distance was 3 to 5 times the lamellar thickness in the regular packing region.

The weak SAXS intensity observed in the amorphous state suggested an inhomogeneity of amorphous structure. From the analysis of correlation function on an absolute scale, a local ordering of atomic configuration was concluded to take place prior to crystallization during ageing. Its region was quantitatively estimated to have an average size of 1.8 to 2.4 nm and have no spherical symmetry.

Acknowledgement

The authors wish to thank Dr S. Takayama for his valuable discussions. They are also thankful to Mr K. Shimomura for his assistance in the experimental work.

References

1. D. E. POLK, *Acta Met.* **20** (1972) 485.
2. S. C. LIN and P. DUWEZ, *Phys. Stat. Sol.* **34** (1969) 469.
3. Y. WASEDA and T. MASUMOTO, *Z. Physik* **B22** (1975) 121.
4. K. SUZUKI, T. FUKUNAGA, M. MISAWA and T. MASUMOTO, *Mat. Sci. Eng.* **23** (1976) 215.
5. T. MASUMOTO and H. KIMURA, *Jap. J. Inst. Metals* **39** (1975) 273.
6. P. K. RASTOGI and P. DUWEZ, *J. Non-Crystalline Solids* **5** (1970) 1.
7. T. MASUMOTO and R. MADDIN, *Mat. Sci. Eng.* **19** (1975) 1.
8. C. C. TSUEI, G. LONGWORTH and S. C. H. LIN, *Phys. Rev.* **170** (1963) 603.
9. C. C. TSUEI and H. LILIENTHAL, *Phys. Rev.* **13** (1976) 4899.
10. F. E. FUJITA, T. MASUMOTO, M. KITAGUCHI and M. URA, *Jap. J. Appl. Phys.* **16** (1977) 1731.
11. C. P. P. CHOU and D. TURNBULL, *J. Non-Crystalline Solids* **17** (1975) 169.
12. J. L. WALTER, D. G. LEGRAND and F. E. LUBORSKY, *Mat. Sci. Eng.* **29** (1977) 161.
13. D. C. BASSETT, A. KELLER and S. MITSUHASHI, *J. Polymer Sci.* **A1** (1963) 763.
14. A. MÜNSTER, "Small-Angle X-Ray Scattering", edited by H. Brumberger (Gordon and Breach, New York, 1967) p. 401.
15. R. HOSEMANN, *Z. Elektrochem.* **58** (1954) 271.
16. G. POROD, *Kolloid Z.* **124** (1951) 83.
17. J. L. WALTER, P. RAO, E. F. KOCH and S. F. BARTRAM, *Met. Trans.* **8A** (1977) 1141.
18. Y. WASEDA, H. OKAZAKI and T. MASUMOTO, *J. Mater. Sci.* **12** (1977) 1927.
19. B. S. GIESSEN and C. N. J. WAGNER, "Liquid Metals", edited by S. Z. Beer (Marcel Dekker, New York, 1972) p. 633.

Received 9 June and accepted 20 July 1978.